On the relationship between $\{11\bar{2}6\}$ and $\{11\bar{2}2\}$ conjugate twins and double extension twins in rolled pure Mg

Andriy Ostapovets[1*], Jiří Buršík[1], Karel Krahula[1], Lubomír Král[1], Anna Serra[2]

[1]*Central European Institute of Technology - Institute of Physics of Materials (CEITEC IPM), Academy of Sciences of the Czech Republic, Žižkova 22, 61662 Brno, Czech Republic*

[2]*Department of Civil & Environmental Engineering, Universitat Politecnica de Catalunya, Jordi Girona 1-3, 08034 Barcelona, Spain*

[*]Corresponding author: tel.: +420 532 290 429, e-mail: ostapov@ipm.cz

Abstract

The paper presents a new type of twin-like objects observed in rolled pure magnesium. They have $\{11\bar{2}6\}$ and $\{11\bar{2}2\}$ habit planes and their misorientations to the matrix are close to 56° and 63° about $\langle 10\bar{1}0\rangle$ axis, respectively. The ad hoc performed theoretical analysis and atomic simulations allow to interpret the objects as $\{10\bar{1}2\}-\{10\bar{1}2\}$ double twins formed by the simultaneous action of two twinning shears with completely re-twinned volume of primary twin. The observed inclinations from the ideal misorientations for such double twins can be explained by the compliance of the strain invariant condition in the twin boundary.

It seems plausible that, once the double twin is formed, its twin boundaries are hard to move by glide of twinning disconnections. If so, these twins represent obstacles for the motion of crystal dislocations increasing the hardness of the metal.

Keywords: magnesium, twinning, grain boundaries, plastic deformation, habit plane.

1.Introduction

Deformation twinning is a frequent phenomenon in metals with hexagonal close packed (hcp) structure such as magnesium, titanium, cobalt and their alloys [1]. Particularly, twinning has a significant contribution to plastic deformation of magnesium. Twinning accommodates deformation along the <c>-axis due to a relative hardness of the non-basal slip in magnesium [2,3]. There are several twinning modes; the most frequent one is the so-called "extension" twinning on $\{10\bar{1}2\}$ twinning plane (K_1) with $\langle\bar{1}011\rangle$ twinning direction (η_1). This mode accommodates extension deformation along the <c> direction in the hcp lattice. The misorientation angle between matrix and twin is 86˚ about $\langle\bar{1}2\bar{1}0\rangle$ axis for $\{10\bar{1}2\}$ twin. The "contraction" twinning accommodates contraction along the <c> direction. The main contraction mode has $\{10\bar{1}1\}$ K_1 plane and $\langle10\overline{12}\rangle$ η_1 direction. Other types of contraction twins were also reported, for instance $\{10\bar{1}3\}$ twinning [1,4,5] or $\{10\bar{1}5\}$ twinning [5]. However, these modes seem to be less frequent than $\{10\bar{1}1\}$ twinning.

Under appropriate circumstances a new twin can be nucleated inside an existing twin. This phenomenon is called double twinning. The most widely reported double twinning modes in magnesium and it alloys are $\{10\bar{1}1\}-\{10\bar{1}2\}$ or $\{10\bar{1}3\}-\{10\bar{1}2\}$ types, i.e. the contraction twinning is followed by the extension twinning [6-10]. Although these modes were studied for several decades, they still attract the attention of scientists. For instance, the influence of double twinning on macroscopic strain was studied recently in [11]. The influence of $\{10\bar{1}1\}-\{10\bar{1}2\}$ double twinning on crack formation and ductility of Mg-Li alloy was analyzed in [12], where it was shown that double twinning does not necessarily lead to cracking.

Less attention has been paid to the extension double twinning of $\{10\bar{1}2\}-\{10\bar{1}2\}$ type. Crocker, in his pioneering theoretical analysis [13], concluded that deformation due to $\{10\bar{1}2\}-\{10\bar{1}2\}$ double twinning cannot be represented as simple shear. Due to this fact, the growth of a extension double twin can be difficult because an additional accommodation of strain is necessary in the twin boundaries. Moreover, the strain produced by the secondary twin in the <c> direction of the matrix is opposite to those produced by the primary one. As a result, $\{10\bar{1}2\}-\{10\bar{1}2\}$ double twins were observed under specific conditions or in complex deformation states such as low temperature compression [14], extrusion and rolling [15] or two-step plastic deformation [16]. In all reported cases of $\{10\bar{1}2\}-\{10\bar{1}2\}$ twinning secondary extension twins were nucleated in large and well developed primary twins. The secondary twins occupy only part of the primary twin volume and are easily distinguished by microscopic observations. This means that the growth mechanism of the secondary twin is the same as the mechanism of the primary twin. The primary twin plays the role of the matrix in this case. However, an alternative scenario of double twin formation is also possible [6,13]. A small primary twin nucleus can be completely re-twinned for the formation of a double twin. Then, the nucleus consequently grows into the matrix and forms a band with the habit plane governed by the combination of shears for primary and secondary twins. In this case, practically the whole volume of the primary twin is re-twinned and secondary twins are not distinguished inside forming really a double twinned region. The growth of such a double twin is mediated mainly by a migration of the boundary between the matrix and the double twin. This kind of $\{10\bar{1}2\}-\{10\bar{1}2\}$ twinning has not been reported yet for magnesium to the best of our knowledge.

The aim of the present paper is to present twin-like objects observed in magnesium.

These objects can be interpreted as $\{10\bar{1}2\}-\{10\bar{1}2\}$ double twins formed by simultaneous acting of two twinning shears as described above.

2. Materials and methods

Magnesium with 99.95% purity provided by MaTecK was used for the observations. Samples with the size of 5×5×20 mm were machined from as received material. Then, the samples were annealed for 0.5h at 300˚C. Coarse grained material with average grain size ~20 μm and maximal size ~80-100 μm was obtained after annealing. Twins were practically absent in the annealed samples. The samples have significant basal texture after annealing as shown by the inverse pole figures in Fig.1a. Then, the samples were rolled at room temperature in order to induce deformation twinning. The sample deformation was +10.2% in rolling direction (RD), -15.7% in normal direction (ND) and +7.2% in transverse direction (TD). Due to the presence of initial texture, the [0001] direction was predominantly oriented along RD before rolling. Consequently, the observed elongation of RD can be easily accommodated by extension twinning. However, the comparable elongation along TD cannot be accommodated by primary $\{10\bar{1}2\}$ twins. This elongation can be accommodated either by slip or by activation of secondary twins inside primary twins. Average grain size after rolling was ~5 μm. The texture after rolling is shown in Fig. 1b. This is typical rolling texture with predominant orientation of <c>-axes nearly-parallel to ND. The inverse pole figures shown in Fig.1 represent typical microtexture obtained from EBSD maps with typical size 500×500 μm (contains about 600 grains) in the case of initial material and 100×100 μm (contains about 2000 grains) in the case of rolled material. The textures obtained from different places on the sample surface

are the same qualitatively. However, some quantitative variation is observed due to relatively small area of each map. Observation by electron-backscatter diffraction (EBSD) method was performed using a Tescan LYRA 3 XMU FEG/SEMxFIB electron microscope equipped with EBSD detector Nordlys Nano by Oxford Instruments. The collection of EBSD data were performed from surface of bulk sample as well as from thin films in transmission EBSD (T-EBSD) mode. The EBSD data were measured with highest camera resolution (1344 x 1024 CCD array) and processed in standard EBSD or TKD indexing mode by AZTEC software by Oxford Instruments. The measured EBSD maps were analyzed in software Channel 5 by Oxford Instruments with low-level noise reduction for bulk samples and without noise reduction for foils. The conventional EBSD was measured under 20kV accelerating voltage with step size 40nm. The specimen was inclined 70º relative to normal incidence of the electron beam. The T-EBSD analysis was done under 30kV accelerating voltage with step size 10 nm. The foil was hold in TKD holder by Oxford instruments. Sample was positioned at an angle 20° relative to normal incidence of the electron beam. Transmission electron microscopy (TEM) was done using a Philips CM12 STEM transmission electron microscope with thermoemission electron source and accelerating voltage of 120kV.

3. Results

3.1 Experimental observations

Abundant twinning was observed in the rolled samples of magnesium. Fig.2a presents an example of EBSD map for selected twinned region. Fig.2b shows the corresponding misorientation angle distribution. Four maxima are observed in the distribution. The first one corresponds to low angle boundaries with angle lower than 10˚.

Another one is quite low characteristic maximum at 30˚ occuring due to CSL boundaries and texture effects [16,17]. High maximum at 86˚ corresponds to $\{10\bar{1}2\}$ twin boundaries. Besides, a quite high maximum at 56˚ is found. The EBSD map (Fig.2a) shows that the 56˚ maximum corresponds to boundaries of plate-like objects, which have twin-like morphology. However, these objects are surprisingly not $\{10\bar{1}1\}$ twins. They have a misorientation of $56^\circ@\langle 10\bar{1}0\rangle$ in contrast to $56^\circ@\langle \bar{1}2\bar{1}0\rangle$ misorientation of the common $\{10\bar{1}1\}$ contraction twins. It is worth noting that the ideal misorientations between matrix and secondary twins are $7.4^\circ@\langle \bar{1}2\bar{1}0\rangle$, $60^\circ@\langle 10\bar{1}0\rangle$ or $60.4^\circ@\langle 8\bar{1}\bar{7}0\rangle$ for different combinations of the variants in $\{10\bar{1}2\}-\{10\bar{1}2\}$ twin. Two of these misorientations are close to the observed one. This fact allows us to suggest that the observed objects are $\{10\bar{1}2\}-\{10\bar{1}2\}$ double twins with completely re-twinned volume of the primary twin. The difference between the observed and the ideal misorientation can occur due to the additional strain accommodation in matrix and twin. However, habit planes of observed objects are significantly inclined from the $\{10\bar{1}2\}$ plane, i.e. the boundary does not lie along the habit plane of the primary twin. TEM observations were performed in order to measure the habit planes of the observed objects. Fig.3a shows the twin with misorientation $56^\circ@\langle 10\bar{1}0\rangle$. It was shown that the habit planes are of $\{11\bar{2}6\}$ type in both, matrix and twin, i.e. the observed boundary is symmetrical. Another example is shown in Fig. 3b, where the misorientation is $61^\circ@\langle 10\bar{1}0\rangle$ with an angle a bit higher than in Fig.3a. The habit planes are close to $\{11\bar{2}2\}$ in this case. However, the majority of observed double twins have misorientation of $56^\circ@\langle 10\bar{1}0\rangle$ and $\{11\bar{2}6\}$ habit planes in our samples (Figs.2,4). The $\{11\bar{2}2\}$ twins were relatively rare in agreement with the misorientation angle distribution shown in Fig.2a. However, the observation of this habit plane supports

the interpretation of considered objects as double twins, as discussed below.

A significant amount of the observed $\{10\bar{1}2\}-\{10\bar{1}2\}$ double twins have the morphology presented in Fig. 4. They are small with length about several micrometers. Such twins are often connected to grain boundaries and terminated inside the grain. The fronts of double twins are sometimes continued as simple $\{10\bar{1}2\}$ twins. Probably, the growth of such double twins can be difficult because reaching the strain compatibility needs additional strain in matrix and twin [13]. The presented morphology agrees with this suggestion. The area fraction of double extension twins is about 3%. This value is obtained by averaging of data for several EBSD maps collected from different Mg samples. Such amount of the twins can indicate that they can play non-negligible role in the process of plastic deformation during rolling.

3.2 Interpretation of $\{11\bar{2}6\}$ and $\{11\bar{2}2\}$ twins as double extension twins

In order to understand the observed results and to prove the interpretation as $\{10\bar{1}2\}-\{10\bar{1}2\}$ double twins, the following calculation of strain compatibility can be provided. Let the deformation gradients due to primary (S_1) and secondary (S_2) twin shears be the following:

$$S_1 = I + s\boldsymbol{m}_1 \otimes \boldsymbol{n}_1 \,, \tag{1}$$

$$S_2 = I + s\boldsymbol{m}_2 \otimes \boldsymbol{n}_2 \,. \tag{2}$$

Here I is the identity matrix, $\boldsymbol{n}$ is the unit vector normal to a shear plane, $\boldsymbol{m}$ is the unit

vector in the shear direction and s is the magnitude of shear. Eqs. (1) and (2) are written relative to the matrix. Let the Q_1 and Q_2 be rotation matrices, which describe misorientations produced by shears S_1 and S_2, respectively. Then the deformation gradient of double twinning can be written as

$$S = Q_1 S_2 Q_1^{-1} S_1 . \tag{3}$$

This deformation gradient is not a simple shear. In order to satisfy the invariant plane condition, additional strain can be suggested. This strain can be taken in the form of a rotation. In practice, such rotation can be provided by disclinations settled in the boundary junctions. Such mechanism was recently discussed in connection to basal-prismatic twin interfaces observed in $\{10\bar{1}2\}$ twins [19,20], where the presence of disclinations allows to change the misorientation across the twin boundary from 86˚ to 90˚. Let Q be the additional rotation due to the disclinations. The invariant twin boundary exists if the deformation gradient QS can be presented in the form

$$QS = I + s\boldsymbol{m} \otimes \boldsymbol{n} , \tag{4}$$

where $\boldsymbol{n}$ is normal to the invariant plane. After application of polar decomposition to S, the Eq. (4) can be rewritten as

$$QQ_sU_s = I + s\boldsymbol{m}\otimes\boldsymbol{n}, \tag{5}$$

where Q_s is rotation, U_s is symmetric matrix and $S= Q_sU_s$. Then, Eq. (5) can be written as

$$Q^*U_s = I + s\boldsymbol{m}\otimes\boldsymbol{n}, \tag{6}$$

by substitution $Q^*=QQ_s$. Eq. (6) is the well known twinning equation [21]. It has solution if the symmetric matrix $C = U_s^2$ has the first eigenvalue λ_1 smaller than 1, the second eigenvalue λ_2 strictly equal to 1 and the third eigenvalue λ_3 higher than 1. If $\boldsymbol{e_1}$ and $\boldsymbol{e_3}$ are the eigenvectors of the matrix C corresponding to the eigenvalues λ_1 and λ_3, respectively, then the two solutions of the Eq. (6) are given by

$$\boldsymbol{m} = \frac{\rho}{\sqrt{\lambda_3-\lambda_1}}\left(\sqrt{\lambda_3(1-\lambda_1)}\boldsymbol{e_1} + k\sqrt{\lambda_3(1-\lambda_1)}\boldsymbol{e_3}\right) \tag{7}$$

$$\boldsymbol{n} = \frac{\sqrt{\lambda_3}-\sqrt{\lambda_1}}{\rho\sqrt{\lambda_3-\lambda_1}}\left(-\sqrt{1-\lambda_1}\boldsymbol{e_1} + k\sqrt{\lambda_3-1}\boldsymbol{e_3}\right) \tag{8}$$

$$s = \sqrt{\lambda_3}-\sqrt{\lambda_1} \tag{9}$$

where $k = \pm 1$, and ρ is chosen to normalize the twin plane normal $\boldsymbol{n}$. The rotation Q^* can be obtained by a direct substitution of the results of Eqs.(7-9) into the equation (6). The resulting misorientation between the matrix and the double twinned region is then defined by the rotation $Q^*Q_1Q_2$.

Table 1 shows habit planes and misorientations provided by the solution of (6). It can be seen that they are in good agreement with the observations and support the interpretation of observed objects as $\{10\bar{1}2\}-\{10\bar{1}2\}$ double twins.

The interpretation of $\{11\bar{2}6\}$ as double twin can be also confirmed by the atomistic simulations shown in Fig. 5. The simulations were performed by using of Liu et al EAM potential [22] for magnesium and LAMMPS [23]. The simulation block was oriented with its x-axis along the normal to $(\bar{1}\bar{1}26)$ plane, y-axis along $[0\bar{2}2\bar{1}]$ direction and z-axis along $[5\bar{3}\bar{2}1]$ direction. Two $\{10\bar{1}2\}$ twin boundaries were inserted into the block and their motion were studied under compression in x-direction.

The simulation shows a migration of two $\{10\bar{1}2\}$ twin boundaries under external stress. The migration of $\{10\bar{1}2\}$ twin boundaries is mediated by $\boldsymbol{b}_{2/2}$ disconnections [20,24], which are aligned with $[0\bar{2}2\bar{1}]$ direction. The term "disconnection" is used for twinning dislocation producing step in the boundary. Such defects are characterized by their Burgers vector and step height. The $\boldsymbol{b}_{2/2}$ disconnections in Fig.5b have Burgers vectors along $\langle 10\bar{1}1\rangle$ directions, i.e. they are of a mixed type in the considered case. Their step height corresponds to two $\{10\bar{1}2\}$ interplanar distances. The interaction of $\{10\bar{1}2\}$ twin boundaries produces a $\{11\bar{2}6\}$ boundary as shown in Fig.5c. This boundary can be interpreted as the boundary between the matrix and the double twinned region if twin T2 is situated inside twin T1.

In principle, simultaneous growth of primary and secondary twins can be equivalent to the new twin modes with K_1 and η_1 provided in Table. 1. Atomistic simulations show lesser mobility of $\{11\bar{2}\bar{6}\}$ boundary in comparison to $\{10\bar{1}2\}$ boundary. The $\{11\bar{2}\bar{6}\}$

boundary stays immobile under a stress level sufficient for initiating the migration of the $\{10\bar{1}2\}$ boundary.

4. Discussion

The most frequent variant of $\{10\bar{1}2\}-\{10\bar{1}2\}$ double twins found in our experiment has a misorientation angle with the matrix equal to 56.8°. This value is a bit different from the ideal misorientations (~60°) for a double extension twin. However, the misorientation angle is close to the misorientation angle of $\{10\bar{1}1\}$ contraction twins (56°). This fact can lead to confusion during interpretation of maxima in the misorientation angle distribution obtained from EBSD. It is necessary to analyze also the misorientation axis in order to distinguish the double twins from $\{10\bar{1}1\}$ contraction twins. The double twin of the considered type seems to be frequent in rolled pure magnesium and can play a non-negligible role in plastic deformation.

Some parallelisms can also be found between double twinning and Type II twin-twin interaction in the terminology used by Yu et al. [25]. The twin T1 in Fig.5 can be considered as a matrix if grains M and T2 in Fig. 5 correspond to two interacting twins, i.e. when T2 is not inside T1. Yu et al. [25] proposed that twin-twin boundaries can be on planes bisecting two twinning planes. These planes are $\{\bar{2}5\bar{3}6\}$ or $\{\bar{1}2\bar{1}2\}$ for Type II(a) and $\{\bar{3}5\bar{2}14\}$ or $\{\overline{13}\ 8\ 5\ 6\}$ for Type II(b) twin interaction. However, Yu et al. [25] agree that the real plane can be different due to the reconstruction undergone to minimize surface energy. The observed that the $\{\bar{1}2\bar{1}2\}$ plane is present in the list proposed in [25] and agree with our analysis of strain compatibility. The $\{\bar{3}5\bar{2}14\}$ proposed by Yu et al. is inclined from $\{11\overline{26}\}$ plane only by 3.7 degrees in the case of magnesium.

It is worth noting that $\{10\bar{1}2\}-\{10\bar{1}2\}$ double twins with $(1\bar{2}16)$ and $(1\bar{2}12)$ habit planes can be considered as a new twinning mode in magnesium. Twins on $\{1\bar{2}12\}$ planes are observed in hcp metals such as Ti and Zr [1]. However, the $\{1\bar{2}12\}$ twinning modes observed in these metals have different shear value from the one listed in Table. 1. Three possibilities for $\{1\bar{2}12\}$ were considered in literature [24]. They can be designated as $\boldsymbol{b}_1$, $\boldsymbol{b}_3$ and $\boldsymbol{b}_4$ according to step height of the disconnection responsible for twin boundary migration in each case. All these modes have twinning direction along $[\bar{1}2\bar{1}3]$. The $\boldsymbol{b}_3$ mode is contraction twin, but $\boldsymbol{b}_1$ and $\boldsymbol{b}_4$ modes are extension twins. The shear values in the case of ideal c/a ratio are 1.22, 0.27 and 0.10 for $\boldsymbol{b}_1$, $\boldsymbol{b}_3$ and $\boldsymbol{b}_4$ modes, respectively [24,26]. The mode observed in Ti and Zr is $\boldsymbol{b}_3$. However, the shear value for $\boldsymbol{b}_4$ mode is 0.112 for c/a=1.624 of magnesium and agrees with the value from Table 1. Moreover, the $\{11\bar{2}\bar{6}\}\langle\bar{1}\bar{1}2\bar{1}\rangle$ twin is conjugate to $\boldsymbol{b}_4$ $\{1\bar{2}12\}$ twin. Therefore, it is possible to conclude that an interaction of two $\{10\bar{1}2\}$ twins can produce a double twin, which is equivalent to $\boldsymbol{b}_4$ $\{1\bar{2}12\}$ twin mode or to $\{11\bar{2}\bar{6}\}$ twin conjugate to it.

The mechanism of $\{1\bar{2}12\}$ twin boundary migration is described in detail in [24,26,27]. However, the migration mechanisms for $\{11\bar{2}\bar{6}\}$ twin boundary were never considered in the literature as far as we know. Nevertheless, the comparison between conjugate $\{11\bar{2}\bar{6}\}$ and $\{1\bar{2}12\}$ twins allows us to speculate about the mobility of their boundaries and about the effect of the observed double twinning on mechanical properties of magnesium.

According to [26] the magnitude of the twinning shear does not determine the core energy of a disconnection. Moreover, its mobility is strongly dependent on the core width, which, in turn, is influenced by the amount of atomic shuffling associated to the step

height. Thus, a core such as the one presented by $\boldsymbol{b}_4$ dislocation, with 4 planes high and large shuffles, should be difficult to move, as was indicated in table 2 of [26]. Consequently, the migration of $\{1\bar{2}12\}$ twin boundary by $\boldsymbol{b}_4$ mechanism is hard in comparison to the migration of common $\{10\bar{1}2\}$ twin boundary. The same can be valid for $\{11\bar{2}\bar{6}\}$ twin, where the correct shear value is also satisfied for $\boldsymbol{b}_4$ disconnection. Fig.6 shows dichromatic complexes for both $\{11\bar{2}2\}$ and $\{11\bar{2}\bar{6}\}$ twin boundaries. The necessary atomic shuffling for $\boldsymbol{b}_4$ mode is shown by red arrows. The complexity of shuffling is comparable for both boundaries indicating that the expected mobility of $\boldsymbol{b}_4$ disconnections are low in both cases.

5. Conclusions

Twins with $\{1\bar{2}16\}$ and $\{1\bar{2}12\}$ habit planes were observed in magnesium. These twins were interpreted as $\{10\bar{1}2\}-\{10\bar{1}2\}$ double twinning with the whole volume of the primary twin re-twinned. Secondary twins are not distinguished inside double twinned plates in contrast to previously reported types of $\{10\bar{1}2\}-\{10\bar{1}2\}$ double twinning.

The most frequent variant of the observed $\{10\bar{1}2\}-\{10\bar{1}2\}$ double twins has a misorientation with matrix $56.8^{\circ}@[1\bar{1}00]$ and habit parallel to $\{1\bar{2}16\}$ planes;

It is proven that $\{1\bar{2}16\}$ twin boundaries can be nucleated by an interaction of $\{10\bar{1}2\}$ twin boundaries.

The observed misorientations between the matrix and the double twin agrees with theoretical predictions, when additional strain accommodations are taken into account in

order to satisfy invariant plane conditions on the twin boundary.

It seems plausible that, once the double twin is formed, its twin boundaries are hard to move by glide of twinning disconnections. If so, these twins represent obstacles for the motion of crystal dislocations increasing the hardness of the metal.

Acknowledgements

This work was supported by Czech Science Foundation under grant 16-14599S; Ministry of Education, Youth and Sports of the Czech Republic under grant CEITEC 2020 (LQ1601); and Spanish MINECO under grant FIS2015-69017-P.

References

[1] J. W. Christian and S. Mahajan, *Deformation twinning*, Prog. Mater. Sci. 39 (1995), pp. 1-157.

[2] A. Chapius and J.H. Driver, *Temperature dependency of slip and twinning in plane strain compressed magnesium single crystals*, Acta Mater. 59 (2011), pp. 1986-1994.

[3] W.B. Hutchinson and M.R. Barnett, *Effective values of critical resolved shear stress for slip in polycrystalline magnesium and other hcp metals*, Scripta Mater. 63 (2010), pp. 737-740.

[4] J. W. Christian, *The Theory of Transformations in Metals and Alloys*, Pergamon Press, Oxford, 1965.

[5] R. Yoshinaga and R. Horiuchi, *Deformation Mechanisms in Magnesium Single Crystals Compressed in the Direction Parallel to Hexagonal Axis*, Trans. JIM 4 (1963), pp. 1-8.

[6] R.E. Reed-Hill, *Study of {1 0 -1 1} and {1 0 -1 3} twinning modes in magnesium,* Trans. Met. Soc. AIME 218 (1960), pp. 554-558.

[7] D. Ando, J. Koike and Y. Sutou, *Relationship between deformation twinning and surface step formation in AZ31 magnesium alloys*, Acta Mater. 58 (2010), pp. 4316-4324.

[8] P. Cizek and M.R. Barnett, *Characteristics of the contraction twins formed close to the fracture surface in Mg–3Al–1Zn alloy deformed in tension*, Scr. Mater. 59 (2008), pp. 959-962.

[9] M.R. Barnett, Z. Keshavarz, A.G. Beer and X. Ma, *Non-Schmid behaviour during secondary twinning in a polycrystalline magnesium alloy*, Acta Mater. 56 (2008), pp. 5-15.

[10] E. Martin, L. Capolungo, L. Jiang and J.J. Jonas, *Variant selection during secondary twinning in Mg–3%Al*, Acta Mater. 58 (2010), pp. 3970-3983.

[11] W. Wu, C.-P. Chuang, D. Qiao, Y. Ren and K. An, *Investigation of deformation twinning under complex stress states in a rolled magnesium alloy*, J. Alloys Compds, 683 (2016), pp. 619-633.

[12] M. Lentz, M Risse, N. Schaefer, W. Reimers and I.J. Beyerlein, *Strength and ductility with {1 0 -1 1}-{1 0 -1 2} double twinning in a magnesium alloy*, Nature Commun. 7 (2016), p. 11068

[13] A.G. Crocker, *Double twinning*, Philos. Mag. 7 (1962), pp. 1901-1924.

[14] J. Jain, J. Zhou, C.W. Sinclair and W. J. Poole, *Double tensile twinning in a Mg–8Al–0.5Zn alloy*, J. Microscopy 242 (2011), pp. 26-36.

[15] A. Jäger, A. Ostapovets, P. Molnár and P. Lejček, *{1 0 -1 2}-{1 0 -1 2} Double twinning in magnesium*, Philos Mag Letters, 91 (2011), pp. 537-544.

[16] Z.-Z. Shi, Y. Zhang, F. Wagner, T. Richerton, P.A. Juan, J.-S. Lecomte, L. Capolungo and S. Berbenni, *Sequential double extension twinning in a magnesium alloy: Combined statistical and micromechanical analyses*, Acta Mater. 96 (2015), pp. 333-343.

[17] A. Ostapovets, P. Molnár and A. Jäger, *Visco-plastic self-consistent modelling of a grain boundary misorientation distribution after equal-channel angular pressing in an AZ31 magnesium alloy*, J Mater Sci 48 (2013), pp. 2123-2134.

[18] A. Ostapovets, P Molnár and P Lejček, *Boundary plane distribution for Σ13 grain boundaries in magnesium*, Materials Letters 137 (2014), pp. 102-105.

[19] A. Ostapovets and R. Gröger, *Twinning disconnections and basal–prismatic twin boundary in magnesium*, Modell. Simul. Mater. Sci. Eng.22 (2014), p. 025015.

[20] A. Ostapovets, J. Buršík and R. Gröger, *Deformation due to migration of faceted twin boundaries in magnesium and cobalt*, Philos. Mag. 95 (2015), pp. 4106-4117.

[21] K.F.Hane and T.W. Shield, *Microstructure in a cubic to orthorhombic transition*, Journal of Elasticity 59(2000), pp. 267-318.

[22] X.Y. Liu, J.B. Adams, F. Ercolessi and J.A. Moriarty, *EAM potential for magnesium from quantum mechanical forces*, Model. Simul. Mater. Sci. Eng. 4 (1996), pp. 293-303.

[23] S. Plimpton, *Fast Parallel Algorithms for Short-Range Molecular Dynamics*, J. Comp. Phys. 117 (1995) pp. 1-19.

[24] A. Serra, D.J. Bacon and R.C. Pond, *The crystallography and core structure of twinning dislocations in hcp metals*, Acta Metall. 36 (1988), pp. 3198-3203.

[25] Q. Yu, J. Wang, Y. Jiang, R.J. McCabe, Nan Li and C.N Tome, *Twin–twin interactions in magnesium*, Acta Mater. 77 (2014), pp. 28-42.

[26] A. Serra, D.J. Bacon and R.C. Pond, *Computer simulation of the structure and mobility of twinning disclocations in HCP metals*, Acta Metall. Mater. 39 (1991), pp. 1469-1480.

[27] A. Serra and D.J. Bacon, *Modelling the motion of twinning dislocations in the HCP metals*, Mater. Sci. Eng. A 400–401 (2005), pp. 496–498.

Figure captions

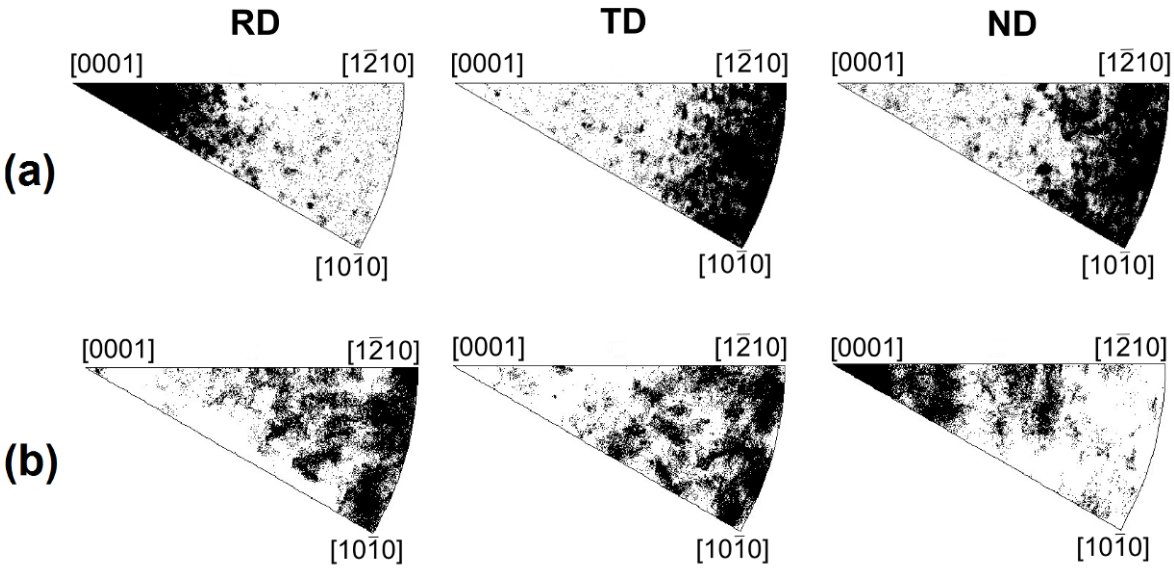

Fig. 1. Inverse pole figures for the initial state of magnesium sample (a) and after rolling (b).

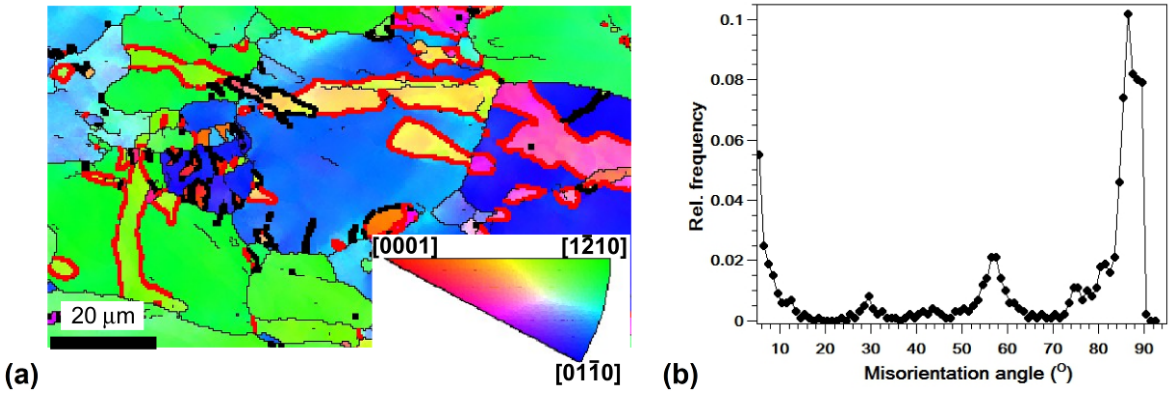

Fig.2. (a) EBSD map of a twinned region in rolled magnesium. Twin boundaries with misorientation $86^{\circ}@\langle \bar{1}2\bar{1}0\rangle$ are marked by thick black lines and boundaries with misorientation $56^{\circ}@\langle 10\bar{1}0\rangle$ are marked by thick red lines. (b) Correlated misorientation angle distribution from the twinned region of magnesium sample.

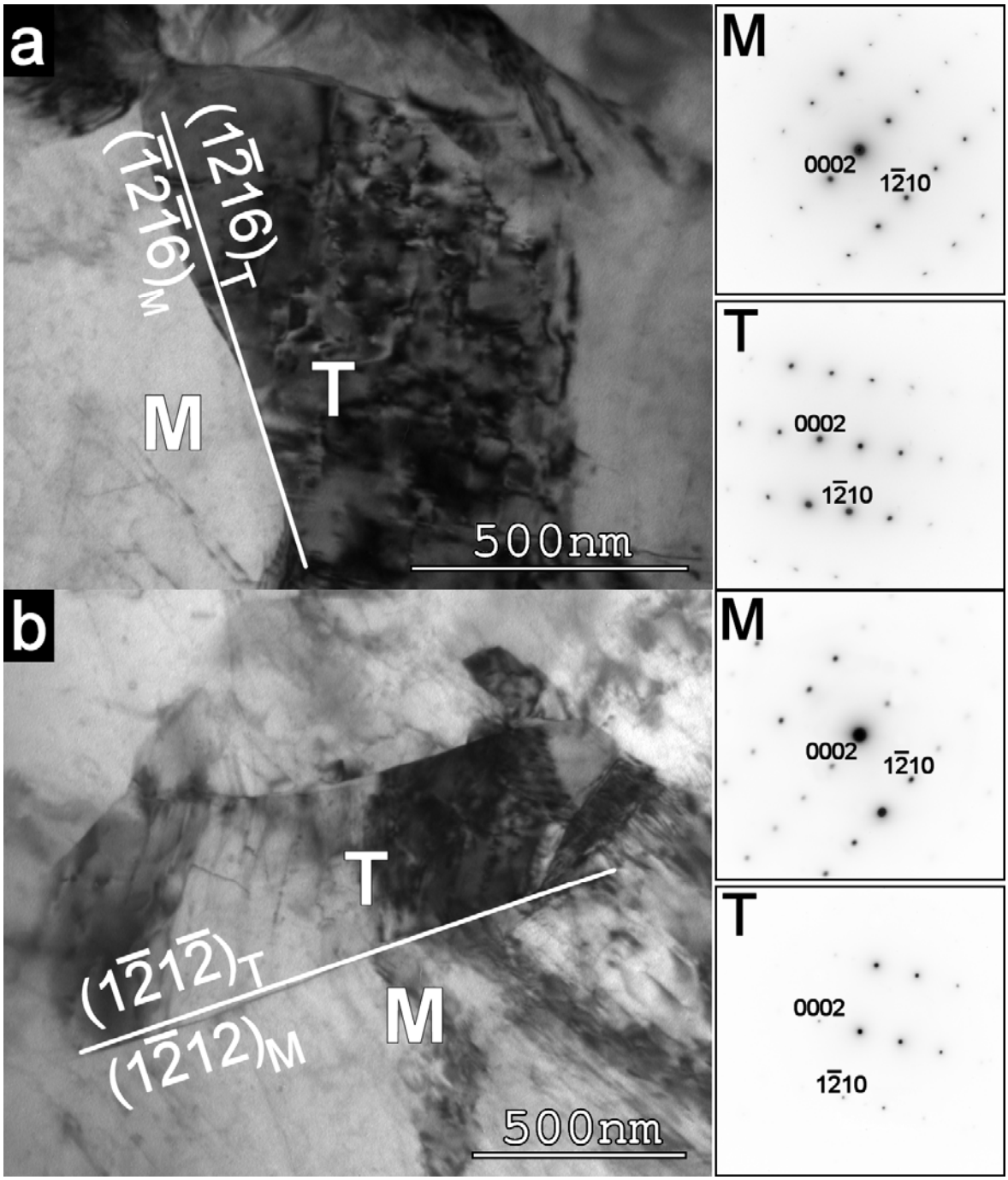

Fig.3. TEM observations of $\{10\bar{1}2\}-\{10\bar{1}2\}$ double twins with $\{11\bar{2}6\}$ habit plane (a) and $\{11\bar{2}2\}$ habit plane (b). M - matrix, T- double twin.

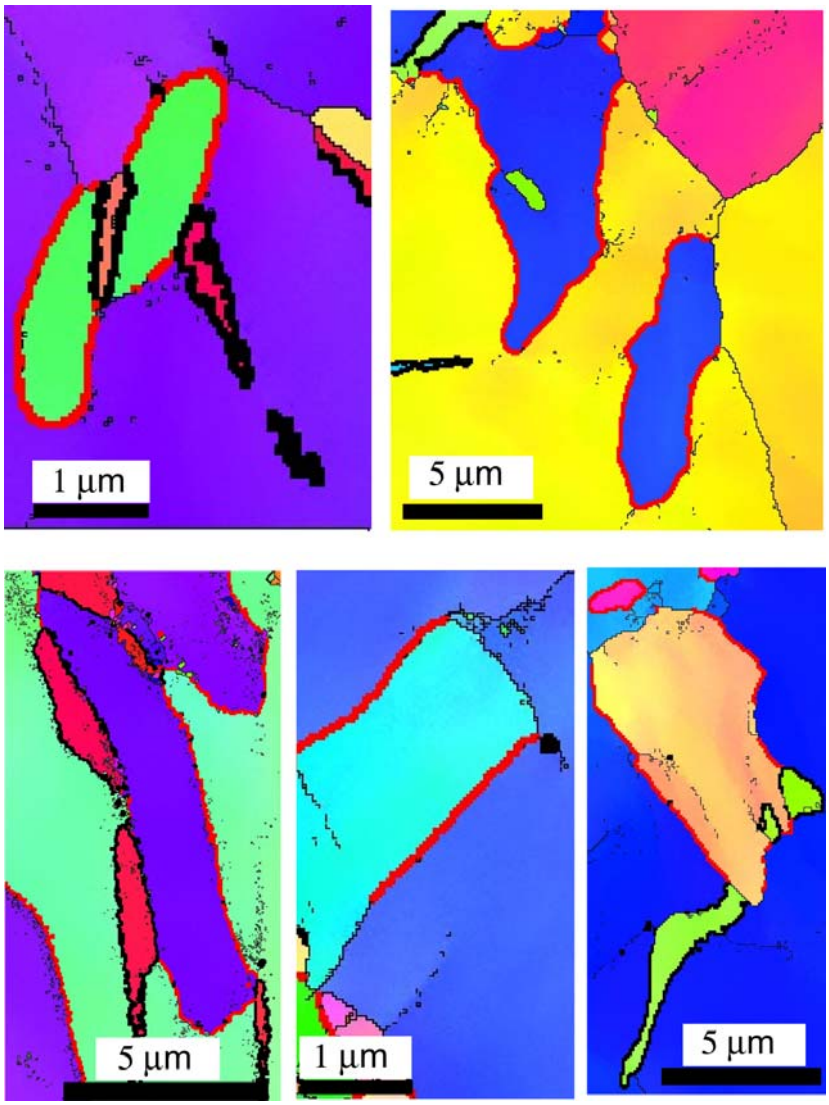

Fig.4. Examples of EBSD maps with $\{10\bar{1}2\}-\{10\bar{1}2\}$ double twins. Boundaries with misorientation $86^{\circ}@\langle\bar{1}2\bar{1}0\rangle$ are marked by thick black lines and boundaries with misorientation $56^{\circ}@\langle10\bar{1}0\rangle$ are marked by thick red lines.

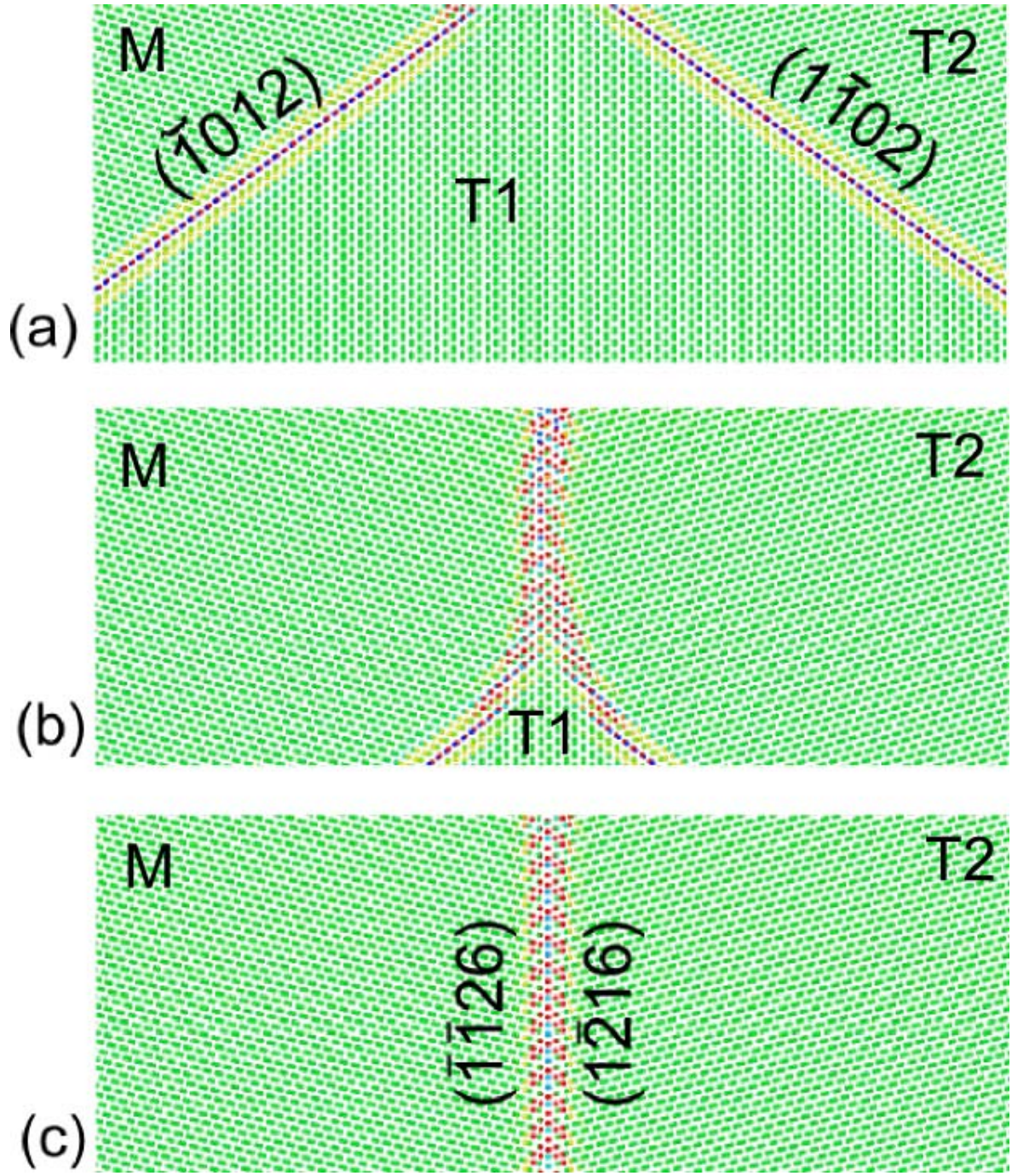

Fig.5. Interaction of two $\{10\bar{1}2\}$ twin boundaries containing common $[0\bar{2}2\,\bar{1}]$ direction. Projection in $[0\bar{2}2\,\bar{1}]$ direction. Initial state (a); intermediate state, where boundaries migrate by motion of mixed 2-layer disconnections (b); final state, where two $\{10\bar{1}2\}$ twin boundaries produce $\{11\bar{2}6\}$ boundary (c).

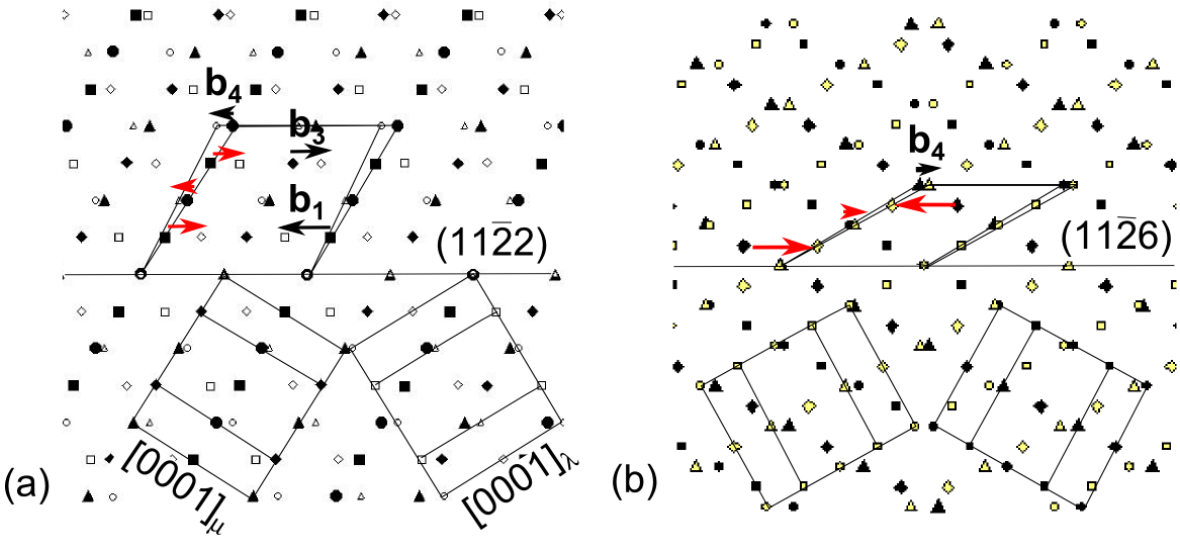

Fig. 6. Dichromatic complexes for $\{11\bar{2}2\}$ (a) and $\{11\bar{2}6\}$ (b) boundaries. The Burgers vectors of disconnections are shown by black arrows. Red arrows show shuffling, which accompanies migration of $\boldsymbol{b}_4$ disconnection.